HGT

Open camera or QR reader and
scan code to access this article
and other resources online.

Identification of Broadly Applicable Adeno-Associated Virus Vectors by Systematic Comparison of Commonly Used Capsid Variants *In Vitro*

Jonas Weinmann,[1] Julia Söllner,[2] Sarah Abele,[1] Gudrun Zimmermann,[1] Kai Zuckschwerdt,[1] Christine Mayer,[1] Jenny Danner-Liskus,[1] Alexander Peltzer,[2] Michael Schuler,[1] Thorsten Lamla,[1] and Benjamin Strobel[1,*]

[1]Drug Discovery Sciences, Boehringer Ingelheim Pharma GmbH & Co. KG, Biberach an der Riss, Germany; [2]Translational Medicine & Clinical Pharmacology, Boehringer Ingelheim Pharma GmbH & Co. KG, Biberach an der Riss, Germany.

Adeno-associated viruses (AAVs) represent highly attractive gene therapy vectors and potent research tools for the modulation of gene expression in animal models or difficult-to-transfect cell cultures. Engineered variants, comprising chimeric, mutated, or peptide-inserted capsids, have strongly broadened the utility of AAVs by altering cellular tropism, enabling immune evasion, or increasing transduction efficiency. In this work, the performance of 50 of the most used, predominantly published, AAVs was compared on several primary cells, cell lines, and induced pluripotent stem cell-derived models from different organs, including the adipose tissue, liver, lung, brain, and eyes. To identify the most efficient capsids for each cell type, self-complementary AAVs were standardized by digital polymerase chain reaction, arrayed on 96-well plates, and screened using high-content imaging. To enable best use of the data, all results are also provided in a web app. The utility of one selected AAV variant is further exemplified in a liver fibrosis assay based on primary hepatic stellate cells, where it successfully reversed a small interfering RNA (siRNA)-induced phenotype. Most importantly, our comparative analysis revealed that a subselection of only five AAV variants (AAV2.NN, AAV9-SLRSPPS, AAV6.2, AAV6TM, and AAV1P5) enabled efficient transduction of all tested cell types and markedly outperformed other well-established capsids, such as AAV2-7m8. These findings suggest that a core panel comprising these five capsid variants is a universally applicable and sufficient tool to identify potent AAVs for gene expression modulation in cellular systems.

Keywords: *ex vivo* transduction, capsid engineering, organoids, neurons, iPSC, immune cells

INTRODUCTION

More than 20 years ago, the first advances in redirecting the tropism of adeno-associated virus 2 (AAV2) were made by creating synthetic capsids with modified surface residues.[1] Since then, many research laboratories working with AAVs have explored, accelerated, and greatly advanced the development of this technology, by steadily engineering novel AAV variants. Three distinct capsid engineering strategies have prevailed over the years, namely (1) introducing point mutations to the *cap* gene sequence by, for example, error-prone polymerase chain reaction (PCR), (2) inserting peptides that are displayed on the surface of the assembled AAV particle, and (3) DNA family shuffling, where parental *cap* gene sequences are

*Correspondence: Dr. Benjamin Strobel, Drug Discovery Sciences, Boehringer Ingelheim Pharma GmbH & Co. KG, Birkendorfer Str. 65, 88400 Biberach an der Riss, Germany. E-mail: benjamin.strobel@boehringer-ingelheim.com

© Jonas Weinmann *et al.*, 2022; Published by Mary Ann Liebert, Inc. This Open Access article is distributed under the terms of the Creative Commons Attribution Noncommercial License [CC-BY-NC] (http://creativecommons.org/licenses/by-nc/4.0/) which permits any noncommercial use, distribution, and reproduction in any medium, provided the original author(s) and the source are cited.

fragmented and subsequently reassembled to generate so-called chimeric capsid variants.

In the first decade of capsid engineering efforts, the focus mainly lay on the development of capsid derivatives with increased transduction efficiencies *in vitro*, resulting in superior AAV vectors in comparison with their respective parental serotypes.[2–11] In the following years, capsid screening campaigns aiming to engineer AAV variants for the transduction of murine tissue *in vivo* were conducted with often great success, best exemplified by capsids such as AAV-PHP.B,[12] AAV2-7m8,[13] and AAVMYO.[14] Advanced xenograft models, such as humanized FRG mice containing human hepatocytes, also led to powerful capsids, with AAV-LK03[15] being the most prominent example. The aspiration to replace the predominately used wild-type AAVs in clinical gene therapy trials with more efficient, specific, and immune-evading synthetic capsids further propelled the ever-growing efforts in developing such tailor-made vectors for future clinical use.

Nowadays, the vast repertoire of AAV vectors allows targeting of many different tissues and cell types in murine models, and recent developments indicate that a similar wealth of efficient capsids for larger animals is also emerging, with the neuron-targeting AAV.CAP-B10 being the latest published example.[16,17]

Besides the evident advantages of utilizing AAVs for gene delivery *in vivo*, AAVs are also very valuable tools for the transduction of cells *in vitro*. Altering gene expression in, for example, primary cells, cell lines, or more complex three-dimensional cell culture models offers the possibility to study cellular effects in a tightly controlled environment. Perhaps most beneficial is the AAV-mediated delivery of genetic payload into cells notoriously difficult to transfect, such as primary cells. In this context, the initial key question usually is which capsid is best suited for efficient transduction. To tackle this question, a comparison of different wild-type AAVs and one engineered vector variant for their ability to transduce primary cells and cell lines was first published by Ellis et al in 2013.[18] On the 34 screened mammalian cell types, AAV2, AAV3, and AAV6 showed the most pronounced transduction rates among the 10 tested capsids.

In a smaller study by Duong et al, AAV1–9 and the peptide-modified vectors AAV2-7m8 and AAV8BP2 (termed AAV8b in the study) were evaluated on induced pluripotent stem cells (iPSCs), iPSC-derived human cortical neurons, iPSC-derived retinal pigment epithelium (RPE), as well as primary rat cortical neurons.[19] AAV6 and AAV2-7m8 exhibited the strongest eGFP reporter expression. In 2020, the *in vitro* comparison of AAVs was further expanded to rationally engineered variants. Börner et al systematically evaluated the performance of rationally designed capsids by integrating 27 previously selected peptides into 13 AAV capsids with remarkable effects.[20] Variants such as AAV1P4 and AAV9A2 demonstrated clear improvements over their parental serotypes in most of the >90 analyzed cell types.

Within the same period, the group of Lisowski utilized the latest advances in genome barcoding to screen a panel of 30 vectors comprising wild types, chimeras, and a few peptide-displaying capsids in 6 cell types.[21] From this barcoded AAV library, the retina-targeting AAV2-7m8 once more showed the overall strongest transcriptional activity.

Sparked by the overwhelming successes of synthetic capsids in those studies, the rationale of this work was to unite all major high-performing engineered vectors, the most used wild-type AAVs, and the latest published variants within one comprehensive AAV panel, thereby allowing an unbiased head-to-head comparison on primary cells and cell lines, including hepatic stellate cells (HepSCs), adipocytes, neurons, iPSCs, and many more. To this end, 50 different AAVs harboring a self-complementary CMV-eGFP-SV40p(A) expression cassette were produced and applied to assess functional transduction by measuring GFP expression. Unlike DNA/RNA-based barcoding, this approach cannot identify functionally defective capsids that enter the cell but do not lead to expression. Yet, as our study was focused on the identification of truly functional capsids, we accepted this limitation and decided for the simple GFP expression-based readout.

As an improvement over the four previous studies, all 36 capsid-modified variants and 14 wild types were fully characterized in terms of production efficiency (measured by droplet digital polymerase chain reaction [ddPCR]), capsid protein expression and purity (sodium dodecyl sulfate–polyacrylamide gel electrophoresis [SDS-PAGE]), as well as viral genome integrity (DNA gel electrophoresis) before screening. Moreover, for the unbiased evaluation of vector performance, equimolar amounts of each variant were used for the transduction before assessing the expression of the eGFP reporter by flow cytometry or high-content confocal imaging. Besides confirming the previously described effects of AAV2 and AAV6 as the most efficient wild types as well as the improvement of AAV1P4, AAV1P5, and AAV9A2 over their parental capsids, we identified the variants AAV2.NN, AAV6.2, AAV9-SLRSPPS, AAV1P5, and AAV6TM as the overall most efficient capsids for *in vitro* use, thereby also markedly outperforming powerful competitors, including AAV2-7m8.

Conversely, the data further provide insights into cell types that are particularly prone to transduction by certain variants, including capsids with generally low *in vitro* efficiency, for example, LX2 cells, which were the only cells strongly transduced by AAV12, and HepG2 cells that allowed robust transduction with AAV3b. Such data might help to identify appropriate cellular systems for capsid

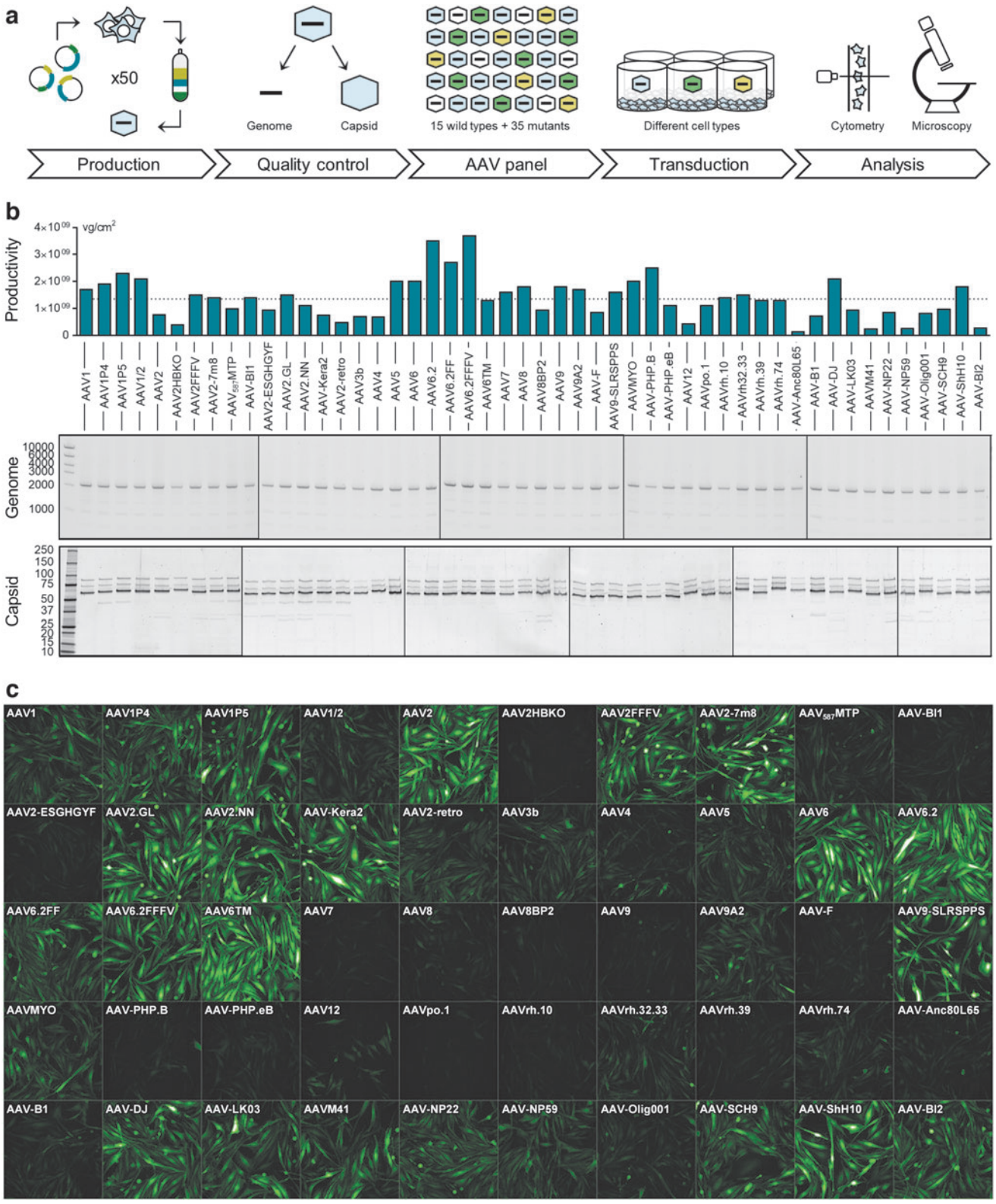

Figure 1. AAV panel: Production, quality control, and screening procedure. **(a)** Workflow of the production and usage of the AAV panel. Fifty AAV capsid variants harboring a CMV-eGFP expression cassette were individually produced and purified over iodixanol gradients. After confirming the quality of all viral batches, vectors were arrayed on 96-well plates and applied for the transduction of various cell types. Following a 1- to 3-day incubation, the percentage of GFP-expressing cells was quantified by high-content confocal imaging and, in some instances, flow cytometry. **(b)** The production efficiency of each AAV variant was determined by ddPCR and is shown as vg per cm^2 of culture area. The *dotted line* indicates the average production efficiency across all batches. AAV genome integrity (expected size: 2,141 bp) was assessed by agarose gel electrophoresis using 1×10^{10} copies of the extracted scAAV genome per lane. Axis labeling: base pairs (*middle panel*). Capsid protein identity and purity were assessed by SDS-PAGE and Oriole staining. Axis labeling: kDa (*lower panel*). **(c)** AAV panel layout and exemplary high-content imaging output for MIO-M1 cells, 3 days after transduction. AAV, adeno-associated virus; ddPCR, droplet digital polymerase chain reaction; sc, self-complementary; SDS-PAGE, sodium dodecyl sulfate–polyacrylamide gel electrophoresis.

development and/or receptor identification campaigns in the future. Therefore, our data alleviate the cumbersome search for efficient capsid variants and foster the use of AAVs to investigate target gene biology in relevant cell culture systems. To enable best use of our findings, all transduction data are also provided in a web app (see exemplary output in Supplementary Fig. S1), which can be accessed through https://aavpanel.boehringer-ingelheim.com

METHODS

AAV production

All 50 AAV batches were produced as described in detail in Strobel et al.[22] Briefly, frozen aliquots of HEK293H cells were thawed and 6×10^7 cells/CELLdisc (Greiner Bio-One) were seeded 3 days before transfection. Adenoviral helper (AAV helper-free system; Agilent), respective rep/cap plasmids, and a plasmid comprising an AAV2-ITR-flanked, self-complementary CMV-eGFP-SV40p(A) expression cassette (see Supplementary Methods in the Supplementary Data for construct sequence) were delivered by calcium phosphate triple transfection. Transfection media of one CELLdisc were changed after 3–4 h and replaced with fresh Dulbecco's modified Eagle's medium (DMEM). After 3 days, cells were detached by the addition of EDTA and were collected by centrifugation. High-salt lysis buffer and three freeze/thaw cycles were used to release the virus particles from the cells. Genomic DNA and remaining plasmids were digested by the addition of salt active nuclease (Serva) before PEG-precipitating proteins, including AAVs, for 3 h.

Following overnight resuspension of the PEG pellet, AAVs were purified over an iodixanol gradient to remove contaminating proteins and empty capsids. The virus-containing iodixanol fraction was concentrated and buffer exchanged using Amicon Ultra-15 filtration tubes (Merck). The concentrate was sterile filtrated, aliquoted, and stored at −80°C for later use.

AAV titration by ddPCR

Viral genomes were isolated with the ViralXpress DNA/RNA Extraction Reagent (Merck) and 5 μL was subsequently serially diluted in nuclease-free H_2O. 9.9 μL of the dilutions 10^{-4}–10^{-11} was transferred to a 96-well plate. Master mix was prepared with 11 μL of 2 × ddPCR Supermix (No dUTP) from Bio-Rad Laboratories and 1.1 μL of 20 × Primer-Probe mix targeting the CMV promoter (forward primer sequence: CCAAGTACGC CCCCTATTGAC, reverse primer sequence: CTGCCAA GTAGGAAAGTCCCATAAG, probe: CCGCCTGGCA TTATG). 12.1 μL of master mix was added to each sample dilution before the 96-well plate was sealed, vortexed, and briefly centrifuged. Center wells of DG8 cartridge (Bio-Rad Laboratories) were filled with 20 μL of sample mix, and 70 μL of droplet generation oil was added to the lower wells of the cartridge. The DG8 cartridge was closed with a rubber band and placed into the QX200 Droplet Generator (Bio-Rad Laboratories).

Upon completion, 44 μL from the upper wells of the cartridge was transferred to a ddPCR 96-well plate. The plate was sealed with a pierceable heat seal foil (Bio-Rad Laboratories) by placing it into the PX1 Plate Sealer (Bio-Rad Laboratories). Afterward, viral genomes were amplified by running a PCR with the following cycling conditions: 95°C for 10 min followed by 40 cycles of 95°C for 30 s and 60°C for 1 min as well as a final step at 98°C for 10 min. Amplicon-containing droplets were measured using a QX200 Droplet Reader (Bio-Rad Laboratories).

Quality control of viral batches

To assess the protein purity of the viral batches, a denaturing SDS-PAGE was performed. Titers determined by ddPCR were used to prepare dilutions of each AAV variant comprising a total amount of 4×10^9 vg in 20 μL. Five microliters of 5 × Pierce™ Lane Marker Reducing Sample Buffer (Thermo Scientific) was added to the 20 μL and samples were heat-denatured at 95°C for 5 min before being loaded on a 4–15% Mini-PROTEAN® TGX Stain-Free™ Protein Gel (Bio-Rad Laboratories). The gel was run at constant 200 V for 30 min and subsequently submerged in 35 mL of Oriole Fluorescent Gel Stain (Bio-Rad Laboratories). Staining was carried out under mild agitation for 90 min at room temperature, then transferred to 35 mL of H_2O, and finally detected by ultraviolet (UV) light.

For visualization of viral genomes, the ViralXpress DNA extracts previously quantified by ddPCR were loaded at a total amount of 1×10^{10} vg in 20 μL of H_2O on a E-Gel™ General Purpose Agarose Gel, 1.2% (Thermo Scientific). 2.05 μL of High DNA Mass Ladder (Thermo Scientific), corresponding to 1×10^{10} copies, was used as a control. Running conditions were fixed to 120 V for 30 min. Afterward, AAV genome bands were visualized by UV light.

Cell culture

Due to the broad repertoire of cells used in this study, culture conditions in this section are limited to the cells shown in Figs. 1–4, while the details for all other cell cultures are available in the Supplementary Data. The human Müller cell line Moorfields/Institute of Ophthalmology-Müller 1 (MIO-M1)[23] was obtained from the UCL Institute of Ophthalmology (London, United Kingdom). MIO-M1 cells were cultured in DMEM high-glucose with GlutaMAX (No. 61965-026; Thermo Fisher) +10% fetal bovine serum (FBS) and seeded at a density of 10,000 cells/96-well 24 h before transduction. Cells were imaged 2 days after transduction. Primary HepSCs were obtained from ZenBio (No. HP-F-S, Lot HSC061218) and cultured in stellate cell medium basal SteCM-b (No. 5301-b; ScienCell/Innoprot) +1 × SteCGS (No. 5352; ScienCell/Innoprot) +2% FBS + GA-1000 in collagen-I-coated flasks.

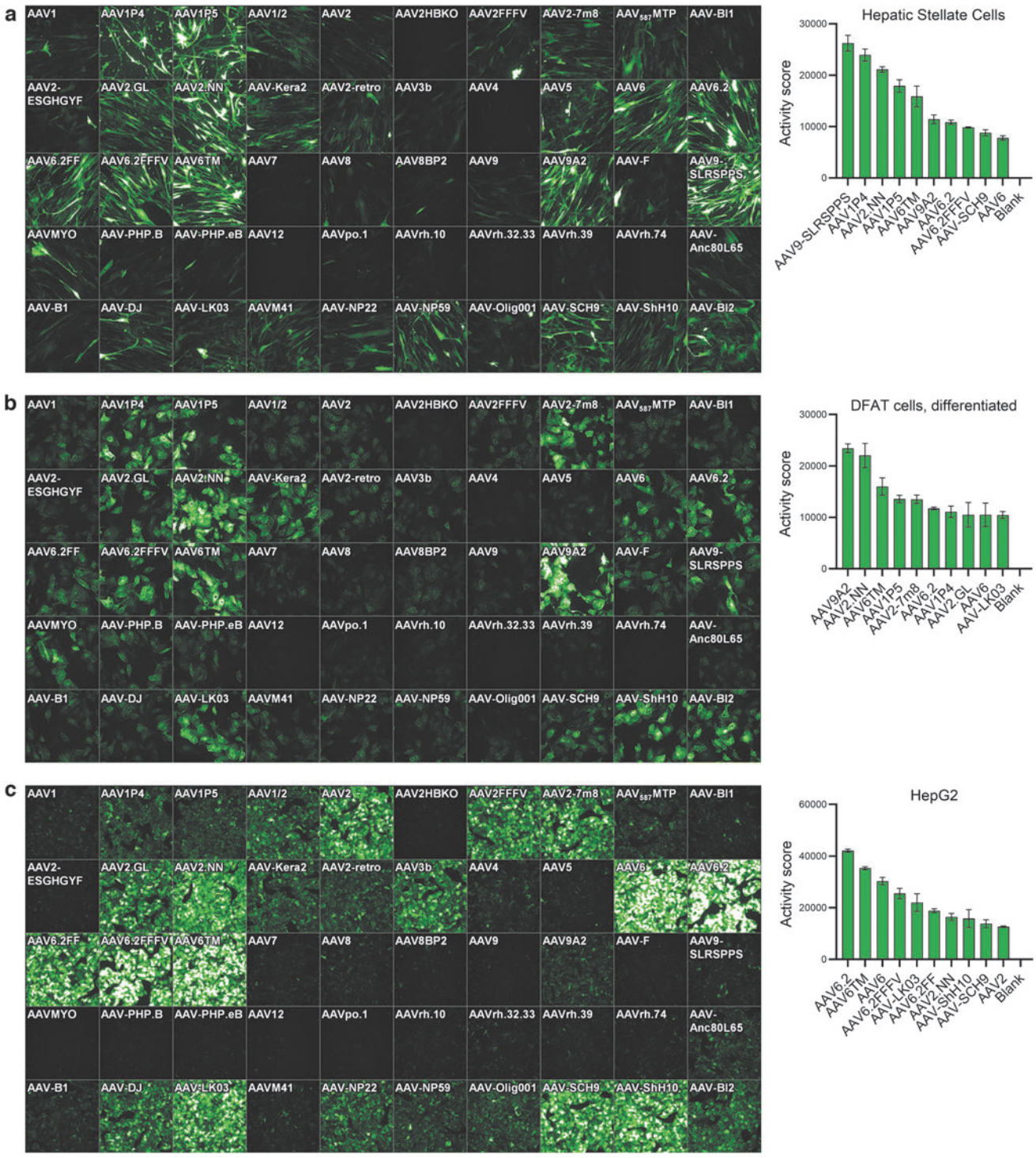

Figure 2. Transduction efficiency on hepatic stellate, differentiated DFAT cells, and HepG2 cells. **(a)** Primary human hepatic stellate cells (11,000 cells/well), **(b)** differentiated primary human DFAT cells (15,000 cells/well), and **(c)** HepG2 cells (50,000 cells/well) were seeded in 96-well plates. Twenty-four hours later, cells were transduced with 2×10^9 vg per AAV variant. Three days later, images were taken by high-content fluorescence microscopy, and GFP-positive cells were quantified by flow cytometry (hep. stellate cells) or semiautomated image analysis (diff. DFAT, HepG2). A ranking of the top performing AAV variants based on the Activity score (%GFP-positive cells × MFI/100) is shown next to each microscopic image. $n=2$ (diff. DFAT) and $n=3$ (hep. stellate cells, HepG2) replicate plates, respectively. Mean ± SD. DFAT cells, dedifferentiated fat cells; MFI, mean fluorescence intensity; SD, standard deviation.

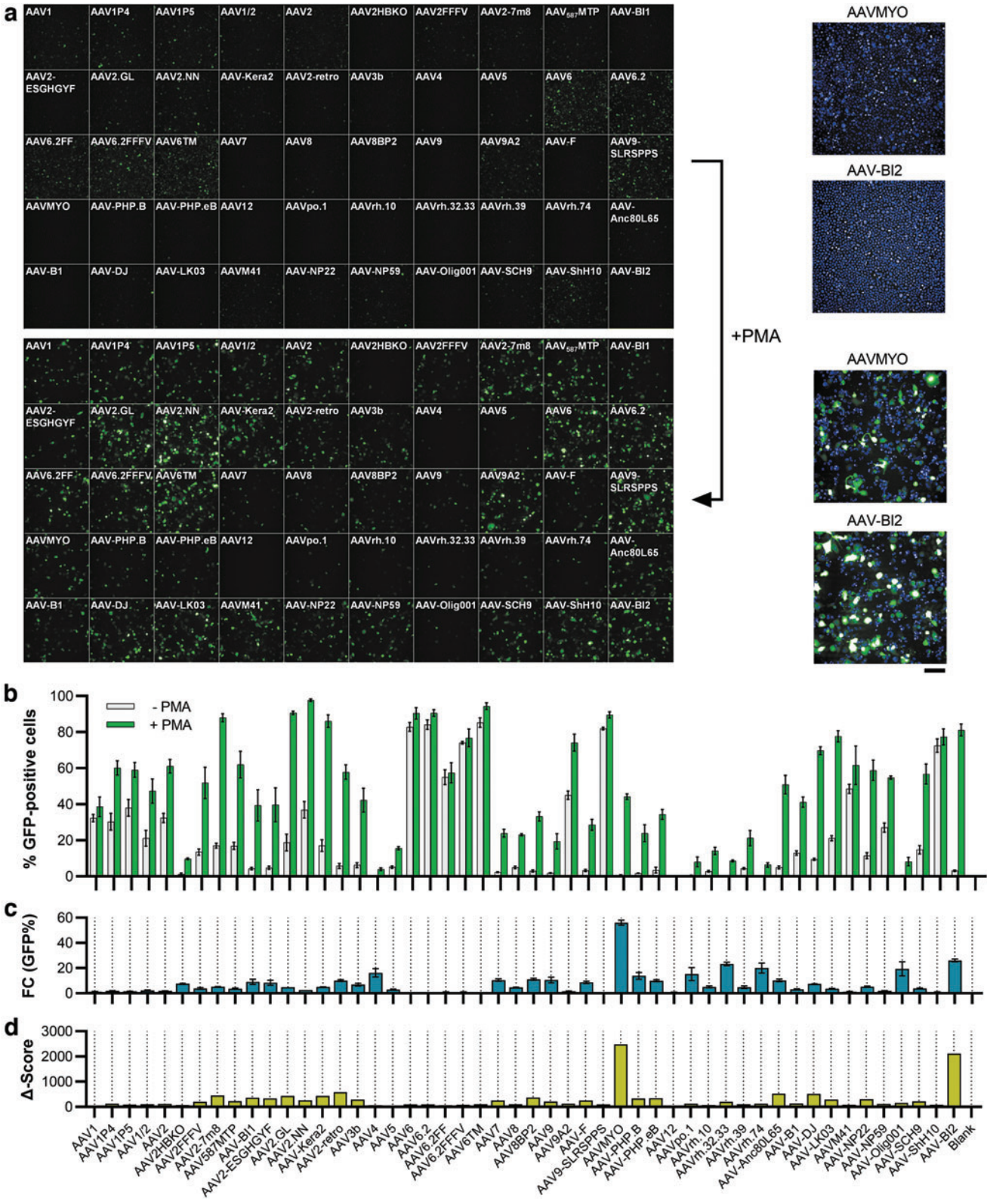

Figure 3. Transduction efficiency on THP-1 cells dependent on PMA stimulation. Sixty thousand THP-1 cells were seeded into 96-well plates and conditionally stimulated with 20 ng/mL of PMA, followed by cultivation in regular media. Twenty-four hours after seeding, cells were transduced with the AAV panel (2×10^9 vg per AAV variant). Three days later, images were taken by **(a)** high-content fluorescence microscopy and **(b)** GFP-positive cells were quantified by semiautomated image analysis. The fold change in the number of GFP-expressing cells between PMA-free and PMA-stimulated conditions is depicted in **(c)** and a composite Δ-score (fold change × %GFP-positive cells) is shown in **(d)**. Enlarged images of the cells transduced with AAVMYO and AAV-BI2 under PMA-free (*top*) and PMA-treated (*bottom*) conditions are shown in the *right part* of **(a)**. *Blue* staining indicates Hoechst33342-stained nuclei. Scale bar = 100 μm. $n = 3$ replicate plates each, mean ± SD. PMA, phorbol 12-myristate 13-acetate.

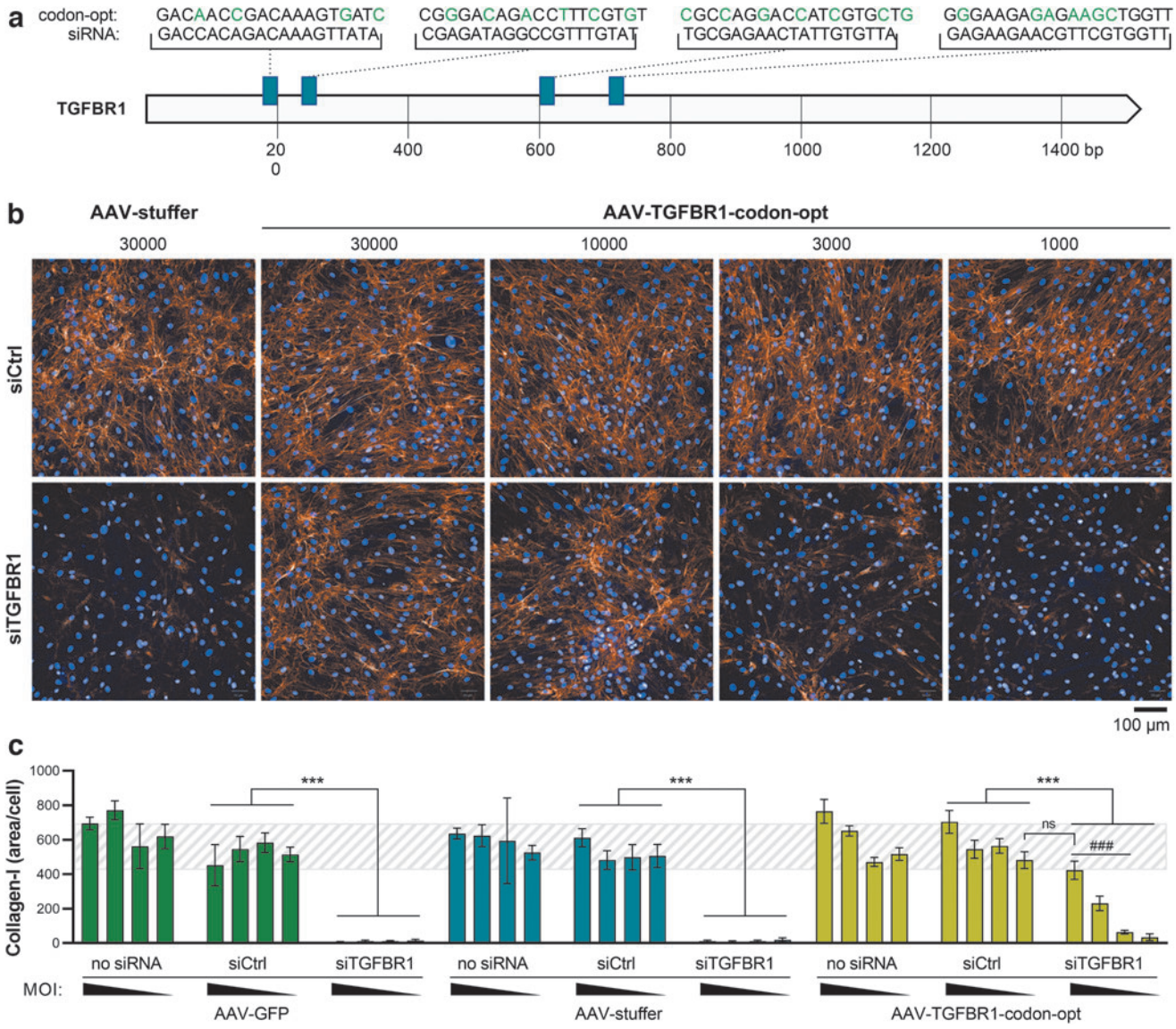

Figure 4. Rescue of fibrotic phenotype in an siRNA-screening assay in human hepatic stellate cells, using AAV9-SLRSPPS. **(a)** An expression construct encoding human TGFBR1 under the control of a CMV promoter was codon-usage optimized ("codon-opt") to escape targeting by the anti-*TGFBR1* siRNA pool (siTGFBR1) and packaged into AAV-SLRSPPS. *Green letters* indicate mismatches between the four siRNAs contained in the pool and the codon-optimized *TGFBR1* sequence contained in the AAV expression construct. Hepatic stellate cells were then reversely transfected with siRNA controls or siTGFBR1 and simultaneously transduced by adding different amounts (1,000, 3,000, 10,000, or 30,000 vg/cell) of either AAV-GFP or noncoding "AAV-stuffer" controls or "AAV-TGFBR1-codon-opt." Collagen-I expression was induced by TGFβ1 (10 ng/mL) and visualized 3 days later by **(b)** immunocytochemistry and **(c)** quantified using a high-content image analysis script detecting nuclei and collagen fibrils. The dashed background indicates collagen-I control levels, defined by the range observed for siCtrl ± SD under AAV-stuffer conditions, for visual guidance. $n=8$ wells/condition, mean ± SD. $^{***}p<0.001$ as indicated. $^{###}p<0.001$ relative to AAV-stuffer. siRNA, small interfering RNA.

Eleven thousand cells/96-well were seeded 24 h before transduction and imaged 72 h later. Primary human dedifferentiated fat (DFAT) cells were isolated from subcutaneous adipose tissue samples (Hepacult), largely as described previously.[24] Briefly, the tissue was dissociated by incubation with 1 mg of collagenase-II solution per mg tissue for 5–10 min at 37°C under gentle agitation followed by filtration through gauze and washing of the cells. Floating cells were then seeded into a culture flask filled with DMEM/F12 + 15% FBS +1% Anti-Anti (No. BE12-719F, Lonza; No. 15240062, Thermo Fisher) and incubated upside down for 1 week to facilitate attachment of the floating cells to the bottom of the flask. For differentiation, cells were cultured in the omental adipocyte differentiation medium (No. OM-DM-500; ZenBio) for 1 week, followed by the omental adipocyte maintenance medium (No. OM-AM-500).

Fifteen thousand cells were seeded for AAV transduction, and GFP-positive cells were quantified 72 h later. HepG2 cells were cultured in MEM with 1% NEAA +10% FBS (Nos. 41090-028, 11140-050; Thermo Fisher) and seeded at a density of 50,000 cells/96-well 24 h before

Table 1. *Capsids of adeno-associated virus panel*

No.	Capsid	Type	Refs.	No.	Capsid	Type	Refs.
(1)	AAV1	Wild type	53	(26)	AAV8BP2	Peptide replacement	54
(2)	AAV1P4	Peptide insertion	20	(27)	AAV9	Wild type	55
(3)	AAV1P5	Peptide insertion	20	(28)	AAV9A2	Peptide insertion	20
(4)	AAV1/2	Mosaic	—	(29)	AAV-F	Peptide insertion	56
(5)	AAV2	Wild type	53	(30)	AAV9-SLRSPPS	Peptide insertion	43
(6)	AAV2HBKO	Point mutant	57	(31)	AAVMYO	Peptide insertion	14
(7)	AAV2FFFV	Point mutant	58	(32)	AAV-PHP.B	Peptide insertion	12
(8)	AAV2-7m8	Peptide insertion	13	(33)	AAV-PHP.eB	Peptide insertion	59
(9)	AAV_{587}MTP	Peptide insertion	60	(34)	AAV12	Wild type	61
(10)	AAV-BI1	Peptide insertion	—	(35)	AAVpo.1	Wild type	62
(11)	AAV2-ESGHGYF	Peptide insertion	63	(36)	AAVrh.10	Wild type	55
(12)	AAV2.GL	Peptide insertion	35	(37)	AAVrh.32.33	Chimera	64
(13)	AAV2.NN	Peptide insertion	35	(38)	AAVrh.39	Wild type	64
(14)	AAV-Kera2	Peptide insertion	65	(39)	AAVrh.74	Wild type	66
(15)	AAV2-retro	Peptide insertion	67	(40)	AAV-Anc80L65	*In silico* design	52
(16)	AAV3b	Wild type	68	(41)	AAV-B1	Chimera	69
(17)	AAV4	Wild type	70	(42)	AAV-DJ	Chimera	71
(18)	AAV5	Wild type	72	(43)	AAV-LK03	Chimera	15
(19)	AAV6	Wild type	68	(44)	AAVM41	Chimera	73
(20)	AAV6.2	Point mutant	39	(45)	AAV-NP22	Chimera	74
(21)	AAV6.2FF	Point mutant	75	(46)	AAV-NP59	Chimera	45
(22)	AAV6.2FFFV	Point mutant	—	(47)	AAV-Olig001	Chimera	76
(23)	AAV6TM	Point mutant	41	(48)	AAV-SCH9	Chimera	77
(24)	AAV7	Wild type	78	(49)	AAV-ShH10	Chimera	79
(25)	AAV8	Wild type	63	(50)	AAV-BI2	Peptide insertion	—

AAV, adeno-associated virus.

transduction, with imaging taking place 2 days later. THP-1 cells were cultured in RPMI 1640 + 10% FBS +1% P/S and seeded at a density of 60,000 cells/96-well. For differentiation, cells were stimulated with 20 ng/mL phorbol 12-myristate 13-acetate (PMA; No. P1585; Sigma) for 8 h and subsequently cultured in regular media. Cells were imaged 72 h after AAV transduction.

AAV transduction

After confirming the purity of the viral batches, virus solutions were diluted with AAV formulation buffer (1 × DPBS, 1 mM $MgCl_2$, 2.5 mM KCl, 10% glycerol, 0.001% Pluronic F-68, pH 7.4, sterile-filtered) to 2×10^8 vg/μL, and 110 μL of the respective dilution was transferred to a 96-well plate consequently creating the AAV panel. Capsid panel plates were stored at −80°C until usage. For the transduction of a cell type, 10 μL of every AAV variant was added to the respective wells of a black ViewPlate-96 (PerkinElmer) harboring the cells. Hence, a total of 2×10^9 vg was used for the transduction corresponding to 100,000 vg/cell in the case of 20,000 cells. Cells were incubated for 3 days at 37°C, 5% CO_2 before measuring the eGFP intensity by microscopy and flow cytometry.

GFP detection by microscopy

To detect GFP-positive cells, ViewPlates were processed with an Opera Phenix High-Content Screening System (PerkinElmer). Five evenly distributed 646 μm^2 fields were measured per 96-well with Brightfield, GFP (excitation at 488 nm, emission at 500–550 nm), and Hoechst33342 (excitation at 405 nm, emission at 435–480 nm) channels. Exposure settings for the GFP channel were fixed to 100 ms and 300 ms for Brightfield and Hoechst33342. Resulting pictures were analyzed with the Columbus Image Data Storage and Analysis System (PerkinElmer). Exposure settings in the software were adapted to HEK293H cells (Xmin = 0, Xmax = 50,000, Xfmid = 0.25) since this cell type exhibited the strongest GFP signals.

In a first step, the Hoechst33342 signal was used to automatically detect vital nuclei. Uneven or overlapping nuclei were excluded by the script. To measure GFP intensities of the vital nuclei area, GFP background signal levels were first determined by quantifying the GFP signal of an untransduced well. Seconf, GFP intensities of vital nuclei areas of transduced wells were measured and averaged to obtain the final GFP intensity score. As an additional readout, percentages of GFP-positive vital nuclei areas were determined for each sample.

GFP detection by flow cytometry

For the quantification of GFP intensity by flow cytometry, cells were washed with 100 μL of 1 × DPBS, afterward detached from the 96-well plate using 30 μL of trypsin-EDTA (Merck) or StemPro™ Accutase™ (Thermo Scientific), and finally mixed with 170 μL of DMEM, 10% FBS. A single-cell suspension was made by pipetting up and down enabling detection with the LSRFortessa™ (BD). Before making measurements, the machine was calibrated using CS&T

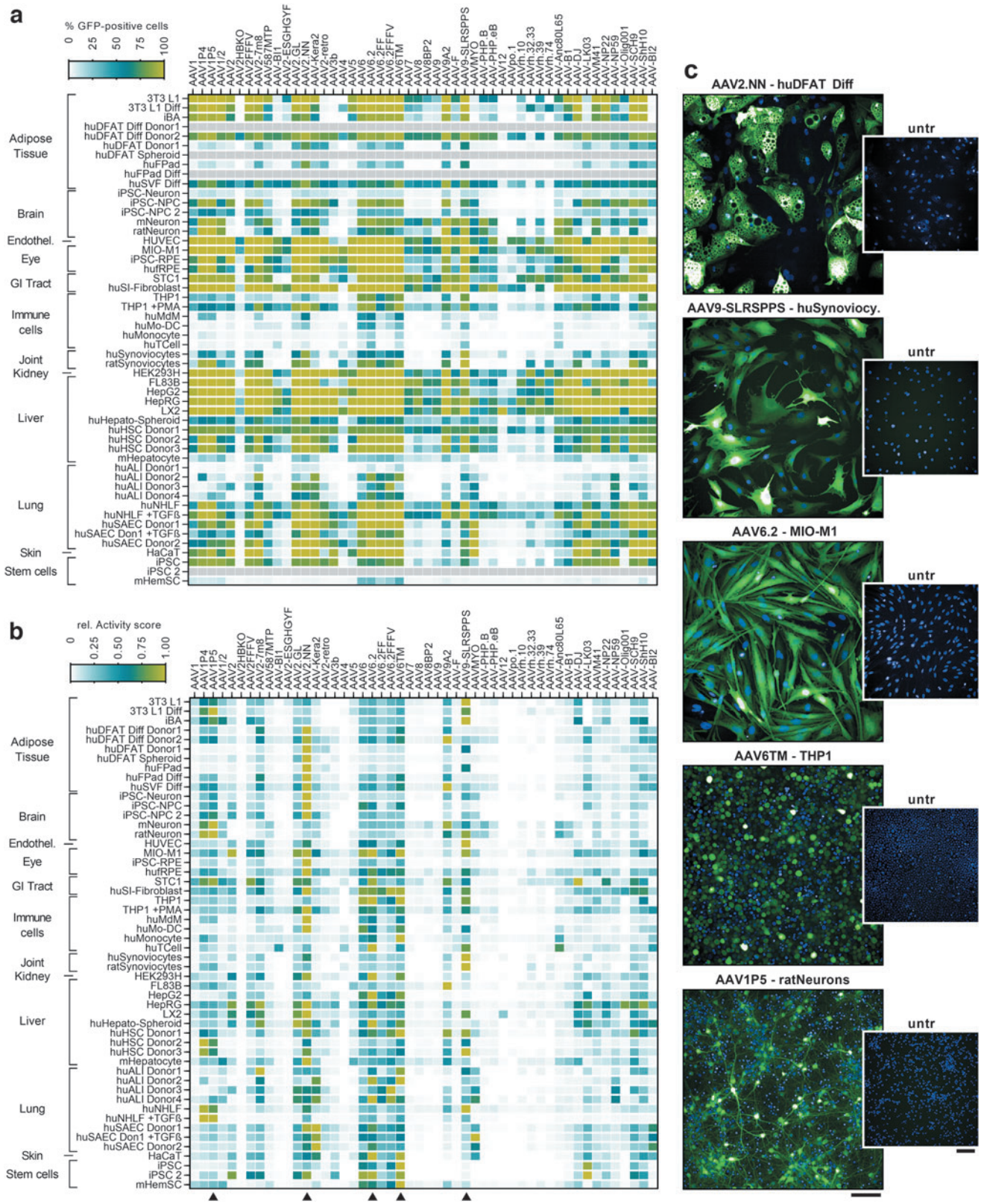

Figure 5. Overview of transduction data and selected application examples for the five AAV core panel variants. **(a)** Heatmap showing the percentage of GFP-positive cells for all 50 AAV variants and transduced cell types, categorized by tissue origin. All cell types and culture methods are described in detail in the Supplementary Data. **(b)** Activity score (% GFP-positive cells × mean fluorescence intensity/100), normalized to the most efficient capsid variant per cell type. The most efficient AAV variant therefore shows a value of 1. *Arrowheads* mark the five capsids selected for the AAV core panel. **(c)** Exemplary micrographs of cells transduced with the AAV core panel variants. Untreated control wells are also shown. *Green fluorescence*: eGFP, *blue* staining: Hoechst33342. Scale bars = 100 μm. hu, human; m, murine.

Research Beads (BD) and by following the instructions in the FACSDiva™ Software (BD). FSC-A against SSC-A depiction allowed separating cellular debris from vital cells and SSC-A against SSC-H was used to differentiate singlets from doublets. Gate for FITC-A was set based on untransduced living singlets, and the percentage of GFP-positive cells as well as mean fluorescent GFP intensities (mean fluorescence intensity [MFI]) were subsequently determined. Values of three replicate 96-well plates were then averaged and standard deviation was calculated.

To address the differences in granularity and size of the tested cell types, forward and side scatter was adjusted accordingly every time. Voltage of the FITC laser was left unchanged for all measurements to guarantee an unbiased outcome.

Collagen assay in HepSCs

For the collagen assay, 4,000 primary HepSCs were reversely transfected with small interfering RNA (siRNA) pools (ON-TARGET Plus siRNA; Horizon Discovery) at a final concentration of 16.6 nM using 0.4 μL of RNAimax in stellate cell medium (SteCM-b [ScienCell/Innoprot] + 1 × SteCGS [ScienCell/Innoprot] + 2% FBS), and simultaneously reversely transduced with different amounts of AAV, as detailed in the results. Twenty-four hours after transfection/transduction, cells were washed and cultured in starvation medium (0.25% FBS) for another 24 h, followed by conditional addition of TGF-β1 (final concentration 10 ng/mL; R&D Systems). Seventy-two hours later, cells were fixed with methanol and stained with Hoechst33342 and an anti-collagen-I antibody (No. SAB4200678; Sigma), as described in detail before.[25] A custom image analysis script[25] was finally used to quantify collagen fibrils and nuclei, thereby enabling calculation of collagen fibrils per cell.

RESULTS AND DISCUSSION

Production and characterization of the AAV panel

To identify the most potent AAV capsids for the transduction of various cell types *in vitro*, we nominated 50 of the most commonly used, largely published AAV variants (Table 1) for an unbiased head-to-head comparison (Fig. 1a). To ensure equal quality of the respective AAV batches, the vectors were produced using a well-established AAV production workflow based on adherent HEK293H cells, followed by AAV purification from cell lysates by iodixanol gradient purification and ultrafiltration.[22] Virus yields were subsequently quantified by ddPCR. The used AAV variants demonstrated varying production efficiencies, with the highest viral genomes per squared cm of culture area (vg/cm^2) observed for AAV6.2, AAV6.2FF, and AAV6.2FFFV and the lowest yields detected for AAV-NP59, AAVM41, and AAV-Anc80L65 (Fig. 1b). Average production efficiency across all 50 variants was 1.35×10^9 vg/cm^2.

Of note, as there are known serotype-dependent differences in the amount of vector particles released to the culture medium,[26] higher yields could probably be achieved for some of the variants by using both lysate and medium for AAV purification. To further characterize the quality of the viral batches, 1×10^{10} vg was loaded onto an agarose gel to visualize the integrity of the viral genome (Fig. 1b). The self-complementary genome was observed at the expected size of 2,141 bp next to faint bands of potentially truncated cargos. The latter observation is in line with recent discoveries that certain structures such as short hairpins in the AAV genome may promote replication stalling, and therefore, a smaller population of diverse cargo variants besides the full-length ITR-to-ITR version.[27–29] Capsid protein purity was finally assessed by Oriole staining of SDS-PAGE gels (Fig. 1b) and revealed the expected VP1, VP2, and VP3 band patterns.

Interestingly, additional bands at ~30 and 50 kDa were observed for the peptide-modified AAV1, AAV2, and AAV8 capsids AAV1P4, AAV1P5, AAV2-7m8, AAV-BI1, AAV2-ESGHGYF, AAV2.GL, AAV2.NN, AAV-Kera2, AAV2-retro, and AAV8BP2. In contrast, no further bands were found for the peptide-modified AAV9 variants AAV9A2, AAV-F, AAV9-SLRSPPS, AAVMYO, AAV-PHP.B, and AAV-PHP.eB. While a detailed investigation of these observations is beyond the scope of this work, the data might point toward differential copurification of host cell proteins or a potential instability/sensitivity of certain peptide display variants in the herein used production system. While the principal propensity of AAVs for protease-mediated capsid cleavage has been described under both artificial (*e.g.*, proteinase K)[30] and process-related conditions (*e.g.*, trypsin[31] used for cell detachment or baculoviral cathepsin in the SF9 production system[32]), these enzymes' involvement can be excluded, given that the AAVs herein were produced in HEK293 cells, and using EDTA instead of trypsin for cell detachment.

Moreover, also differential thermostability of natural AAV serotypes is well documented,[33,34] with two recent studies further indicating lower melting points for AAV2.GL, AAV2.NN, and other AAV2-based peptide insertion variants.[35,36] However, while peptide insertions *per se* as well as lower capsid thermostability can impact several aspects of AAV biology, including genome packaging, cellular binding/uptake, intracellular transport, and genome release,[35,37,38] it has (to our knowledge) not been investigated whether altered thermostability (with melting points >50°C) is predictive for a capsid's susceptibility to stressors and fragmentation at temperatures faced during vector production (≤37°C). Additional experiments are therefore required to explain the occurrence and identity of the protein bands observed besides VP1–3 in Fig. 1b.

After titrating all 50 AAV vector batches and performing the aforementioned quality control steps, equal amounts of all variants were arrayed on 96-well plates and stored at −80°C until use. For all upcoming transduction efficiency screenings, target cells were seeded in 96-well plates and transduced by adding 10 μL (2×10^9 vg) of the AAV panel variants per well.

As a reference for all experiments, HEK293 cells were transduced and analyzed, first (see web app and Fig. 5). To allow for direct comparability of GFP fluorescence intensity across all tested cell types, high-content imaging parameters were set using HEK293 cells and then used for all other measured cell types. Figure 1c shows the layout of the AAV panel and an exemplary GFP micrograph of the Müller glia cell line MIO-M1 upon transduction. The data clearly show strong differences in both the various AAVs' transduction efficiency and the GFP expression intensity mediated by the vectors in these cells. To quantify the percentage of GFP-positive cells and the MFI of GFP signal, semiautomated image analysis was applied.

Supplementary Figure S1 shows an exemplary output of the web app that was designed to enable access to the results of all screened cells, including GFP micrographs and quantitative expression data. In addition to the percentage of GFP-positive cells and the GFP MFI, also a combined ''Activity score,'' calculated by multiplying the % GFP-positive cell value with the GFP fluorescence intensity (% GFP-pos. × MFI/100) is reported. The Activity score is a simple composite measure for overall capsid performance, integrating both transduction efficiency and the degree of transgene expression mediated by a given capsid. It is also useful to rank powerful capsids in instances, where the used AAV dose led to 100% transduction efficiency and probably multiple transduction events per cell.

Due to the interactive setup of the web app, all quantitative readouts can also be automatically sorted to rapidly identify the best performing AAV variants (Supplementary Fig. S1b), which in case of MIO-M1 were AAV6.2, AAV6TM, and AAV2.NN. AAV6.2 is a point-mutated (F129L) variant of AAV6 that was initially described for the transduction of primary human airway epithelial cells[39] and is also one of the most powerful AAVs for lung epithelial transduction in mice.[40] AAV6TM contains three mutations of two surface-exposed tyrosine and one threonine residue (Y705F, Y731F, T492V) over AAV6, and was shown to effectively transduce hematopoietic stem/progenitor cells (HSCs) *ex vivo*,[41] a finding that was also confirmed in our analyses (see web app and Fig. 5).

Finally, AAV2.NN is a recently published, AAV2-based peptide insertion (NNPTPSR) variant that was isolated using a systemic, retina-focused selection approach in mice and turned out to broadly transduce all retinal layers, including photoreceptors, in mice, dogs, and nonhuman primates upon intravitreal administration.[35]

Transduction of liver and adipose tissue cells

Cell culture models of liver and adipose tissue are of interest to study potential target genes, pathways, and biomarkers in the context of obesity and nonalcoholic steatohepatitis (NASH) drug discovery research, as well as for (cardio-)metabolic gene therapy approaches. Our analyses therefore also included several cell types with relevance for these indications, for example, hepatocytes, stellate cells, fat cells differentiated toward white or beige/brown phenotypes, and immortalized brown adipocytes.[42] AAV transduction efficiency for three of those cell types, that is, primary human HepSCs, differentiated human DFAT cells, and the hepatocyte cell line HepG2, is shown in Fig. 2. For HepSC, many variants showed efficient transduction, with AAV9-SLRSPPS—a peptide-inserted AAV9 variant that was selected on human coronary endothelial cells[43]—displaying the highest Activity score.

The following five AAVs in the rank order again contained AAV2.NN and AAV6TM, but also three peptide-insertion variants published by the Grimm laboratory, that is, AAV1P4 (peptide: NDVRSAN), AAV1P5 (NDVRAVS), and AAV9A2 (NYSRGVD), all of which markedly outperformed their parental capsids. Interestingly, the P4 and P5 peptides also originate from a selection on endothelial cells,[7,20] similar to SLRSPPS.

In adipocytes generated by differentiation of primary human DFAT[24] cells, an overall similar transduction pattern was observed, with AAV9A2 and AAV2.NN being the most efficient variants (Fig. 2b), followed by AAV6TM, AAV1P5, and AAV2-7m8, which was previously found to be one of the best performing AAVs in various cell types *in vitro*.[21] In contrast, AAV9-SLRSPPS only showed low expression in DFAT cells. Very similar results were also observed for a second DFAT donor (with AAV2.NN being the top hit) as well as other cellular fractions isolated from adipose tissue (Fig. 5).

Finally, HepG2 cells displayed very effective transducibility (Fig. 2c), as evident from the strong and partly oversaturated GFP signal (with the latter being a result of choosing identical AAV amounts and exposure times for all tested cell cultures for reasons of comparability). On HepG2, the AAV6 family showed most efficient transduction, led by AAV6.2. Of note, the human hepatocyte-selected AAV-LK03 variant[15] was similarly efficient, and AAV3b, a wild-type capsid that rarely shows efficient transduction *in vitro*, also displayed strong effects in these cells, in line with its largely human liver cell-restricted tropism.[44] In contrast, AAV-NP59, which was also described for human liver transduction,[45] showed weaker expression. These results give some insight into the difficulties associated with choosing cellular models predictive of *in vivo* tropism. Still, the results might suggest suitability of HepG2 cells as an intermediate filter or a preselection step in capsid engineering cascades aiming for human liver transduction.

AAV transduction of adherent versus suspension cultures

While testing various cell types for their amenability to AAV transduction, also marked differences between cell types in suspension and adherent culture were observed. For instance, the human monocytic cell line THP-1 was transduced both in suspension culture and following differentiation using PMA, upon which the cells differentiate into a macrophage-like phenotype, which is accompanied by attachment to the culture plates (Fig. 3). When analyzing the transduction data, several AAV variants achieved high and similarly efficient transduction rates in both suspension and adherent cultures, with AAV6, AAV6.2, AAV6TM, AAV9-SLRSPPS, and AAV-ShH10 showing more than 80% GFP-positive cells under both conditions (Fig. 3a, b). In contrast, some AAVs only showed very low transduction in suspension, but drastic increases in the differentiated state, upon cell attachment (Fig. 3b). Respective changes are illustrated as the fold change in the percentage of GFP-positive cells in Fig. 3c.

To correct for the effect that some variants showed high fold changes but still very low numbers of GFP-positive cells (which was observed *e.g.*, for AAV4, the rhesus isolates and AAV-Olig001), the fold change in %GFP-positive cells was further multiplied with the absolute percentage of GFP-positive cells in the differentiated state to calculate the so-called Δ-score (Fig. 3d). This score allowed for the rapid identification of AAV variants whose changes between suspension and adherent culture were strong but also meaningful in terms of overall efficiency. Strikingly, the two top hits were AAVMYO and the variant AAV-BI2, both of which harbor the identical, integrin binding motif-containing RGDLGLS peptide.

These results clearly suggest that the observed increases in transduction efficiency (from 0.8% to 44.2% and 3.1% to 81.2%, respectively) are mediated by integrins that are upregulated upon cell attachment. Besides this obvious RGD motif-mediated effect, many other AAV variants also showed varying degrees of transduction enhancement in adherently growing cells, whereas others, for example, AAV1 and AAV6-related vectors, including AAV-ShH10 did not display any differences (Fig. 3b, c). The observation that also the AAVR-independent[46]serotypes AAV4 and AAVrh32.33 displayed respective increases makes it unlikely that altered AAVR expression is the explanation for this finding. However, a plausible hypothesis is that PMA directly impacts AAV transduction, similar to several other small molecules that were identified as AAV transduction enhancers by the Samulski group.[47] Of note, PMA is a known inducer of macropinocytosis,[48] a process whose inhibition was demonstrated to modulate AAV cellular entry in a cell-type-dependent manner.[49]

These results demonstrate that the AAV panel, in addition to its utility for the identification of potent AAVs, can also be used to shed some light on receptor usage and cellular properties that may conditionally confer amenability to the transduction by certain AAV variants. Possible applications in that regard include transduction experiments on cells under healthy and (induced) pathological conditions, possibly combined with proteomic analyses to examine receptor deregulation.

Rescue of fibrotic phenotype in an siRNA-screening assay in human HepSCs

As outlined above, AAVs capable of transducing primary human cells with high efficiency are valuable tools for early drug discovery research. In the context of metabolic diseases, obesity, fatty liver disease, and NASH are diseases with high prevalence, therefore representing focus areas for the development of new therapeutic treatments. In fact, there is also a clinical link between these diseases, as obesity represents a risk factor for nonalcoholic fatty liver disease and resulting pathologies including NASH and liver fibrosis.[50] To identify and validate targets that drive fibrogenesis, our group has previously developed a high-content imaging-based phenotypic assay based on TGFβ1-induced collagen-I expression.[25,51] In addition to primary lung fibroblasts and airway epithelial cells in the original publication, this assay has meanwhile been expanded to primary HepSCs.

In this study, HepSCs are transfected with siRNAs targeting a protein/transcript of interest, stimulated with TGFβ1 and subsequently stained for collagen-I. Target candidates whose knockdown exerts potential antifibrotic effects are therefore characterized by a lowered profibrotic collagen deposition in those cells.

As a positive control, a pool of four siRNAs, targeting TGFβ receptor 1 (TGFBR1) (Fig. 4a), is routinely applied, thereby disrupting profibrotic TGFβ1 signaling and preventing collagen deposition (Fig. 4b, c). However, the ability to rescue fibrogenesis by reconstituting expression of siRNA-depleted genes would be an attractive feature in this assay, especially to validate potential hits and to characterize poorly explored novel targets. We therefore screened the AAV panel on HepSCs and found AAV9-SLRSPPS to result in a transduction efficiency of up to 98% (Fig. 2a). Using this vector, we then expressed—as a proof-of-concept—a *TGFBR1* variant that was codon-usage optimized to escape targeting by the cotransfected anti-*TGFBR1* siRNAs (Fig. 4a).

To this end, HepSCs were reversely transduced and transfected by mixing the cells with increasing amounts of AAV (1,000, 3,000, 10,000, 30,000 vg/cell) and the siRNA pool, respectively, before seeding into multiwell culture plates. Following starvation and subsequent stimulation with 10 ng/mL of TGFβ1, the cells were incubated for 48 h, stained with Hoechst 33342 to visualize nuclei as well as a fluorescent anti-collagen-I antibody, and imaged on an Opera Phenix system (Fig. 4b). Collagen fibrils were identified by an automated image analysis and normalized to the number of nuclei (*i.e.*, cells) per well (Fig. 4c).

Notably, while treatment with the anti-*TGFBR1* siRNA resulted in the expected blockage of TGFβ-induced collagen expression, AAV-mediated coexpression of codon-altered TGFBR1 successfully rescued the fibrotic phenotype in a dose-dependent manner (Fig. 4b, c).

In contrast, control-AAVs containing either a GFP reporter gene or noncoding DNA (''AAV-stuffer'') did not increase collagen expression. Interestingly, under conditions where endogenous TGFBR1 expression was maintained (*i.e.*, no siRNA or siCtrl), AAV-TGFBR1 increased collagen deposition beyond the levels observed with AAV control vectors, indicating that supraphysiological TGFBR1 availability can enhance the overall level of collagen.

In summary, AAV-mediated rescue of siRNA-depleted TGFBR1 clearly enabled restoration of the pathological phenotype, thereby building the basis for the profiling and validation of NASH-relevant targets in this primary cell-based assay.

Intercellular comparison and identification of a core AAV panel sufficient for transduction of all tested cell types

Finally, the transduction data collected for all cell types across tissues were compiled and visualized in Fig. 5a (% GFP-positive cells) and Fig. 5b (relative Activity score), rapidly confirming the known and highlighting several novel findings: First, tissue-derived cells are transduced at much higher efficiencies than immune and stem cells, which is a well-known fact for AAVs. An exception are the AAV6 family members AAV6.2 and AAV6TM, which achieve decent transduction rates in immune and hematopoietic stem cells, in line with the original publication for AAV6TM.[41] In contrast, AAV6.2FF and AAV6.2FFFV (which combine the mutations of 6TM and FF) did not show any obvious superiority over parental AAV6 in most cell types.

Second, some engineered AAV variants are largely inefficient *in vitro*, including the heparin binding domain-depleted AAV2HBKO, the lung endothelium-tropic AAV2-ESGHGYF, the retinal bipolar cell-targeting AAV8BP2, and the blood–brain barrier-crossing PHP variants. The Anc80L65 variant was also largely inefficient and additionally characterized by very low production yields, which had also been observed by the authors of the original study[52] (Fig. 1b). Similarly, several wild types only showed low or moderate overall efficiency, including AAV4, AAV7, AAV8, AAV9, AAV12, AAV.po1, AAVrh.10, and AAVrh.74. For this reason, particularly notable findings were the significant transduction efficiency of AAV3b in HepG2 cells, and that of AAV12 in the HepSC line LX2 (Fig. 5a). In this study, AAV12, in stark contrast to all other cell types, showed remarkably strong expression, potentially providing an interesting starting point for the identification of the receptor mediating this effect.

Third, the AAV-LK03 variant, a chimeric capsid selected for human hepatocyte transduction, emerged as the best capsid for the transduction of iPSCs, a cell type notoriously difficult to be engineered by AAVs. Additional experiments to characterize LK03's utility in this context are currently ongoing in our group. The last major and most important finding of our study is the identification of AAV variants that showed very broad transduction efficiency, largely independent of the tissue origin of transduced cells.

These data demonstrate that a selection of only five capsids, AAV2.NN, AAV9-SLRSPPS, AAV6.2, AAV6TM, and AAV1P5, is sufficient to identify highly efficient capsids for all tested cell types, exemplary images of which are shown in Fig. 5c. Therefore, a lean ''core panel'' comprising these five AAV variants could be used in the future to identify potent *in vitro* tool capsids. Such a core panel could also easily incorporate serial vector dilutions to enable capsid comparison across different doses as well as rapid identification of the most suitable vector dose for a given cell type.

The broadest efficiency and the highest number of top rankings showed AAV2.NN, an only recently identified, AAV2-based NNPTPSR peptide insertion variant, which was isolated in a retina-focused screening and showed highly efficient transduction upon intravitreal administration in mice, dogs, and nonhuman primates.[35] Interestingly, despite their focus on retinal transduction and in contrast to most other capsid selection approaches, the approach of Pavlou et al was based on systemic delivery of the AAV library and recovery of viral genomes only 24 h after administration. While it is unclear whether this stringent selection process is the reason for this capsid's superior performance, it is certainly noteworthy, especially as AAV2.NN seems to achieve high transduction efficiencies already at a relatively low vg/cell (ongoing work, data not shown). Its higher potency also often compensates for its lower production efficiency, compared with other high performers, for example, AAV6.2 (Fig. 1b).

Another efficient capsid in our comparative analysis was AAV9-SLRSPPS, initially selected by Oliver Müller's laboratory for endothelial transduction.[43] In line with the original finding, our data confirm this variant's strong efficiency on human umbilical vein endothelial cells (Fig. 5), where it was superior to all other tested capsids, including the parental AAV9. Interestingly, it was also the most efficient capsid in HepSCs, normal human lung fibroblasts (NHLF), and synoviocytes (Fig. 5c), all of which are of mesenchymal origin. Similar to AAV9-SLRSPPS, AAV1P5 was also built by incorporation of an endothelial-targeting peptide, NDVRAVS.[7,20]

Overall, AAV1P5 showed a very similar transduction pattern as AAV9-SLRSPPS, however, in some instances, for example, mouse- and rat-derived cortical neurons (Fig. 5c), it led to higher expression levels, justifying its nomination for the core panel. Moreover, also AAV9A2, another variant from the Grimm laboratory, was particularly efficient in neurons and additionally standing out in FL83B, a liver cell line useful for preclinical studies due to its murine origin.

Last, the AAV6 variants AAV6.2 and AAV6TM showed a remarkably broad efficiency across many cell types of different origins. Of note, also immune cells, which in general are difficult to transduce using AAVs, were transduced at a relatively high efficiency, including monocyte-derived dendritic cells and macrophages as well as the monocytic cell line THP-1 (Fig. 5c). AAV6TM further transduced murine HSCs, confirming the original publication,[41] and human iPSCs. Given that AAV6.2 and AAV6TM only harbor one (F129L) and three (Y705F, Y731F, T492V) mutations, respectively, compared with the parental AAV6 capsid, these data also nicely illustrate how small defined changes to a capsid can have a major impact on its performance.

Yet, despite the convincing effects on various tested cell types *in vitro*, a similar *in vivo* performance of the five core panel variants and all other herein tested AAVs cannot be easily extrapolated. This is, among others, due to the increased complexity of *in vivo* systems, including biodistribution across several cellular barriers, an often-pronounced liver transduction of many AAV variants, and differential receptor expression between natural and cell culture conditions. *Vice versa*, capsids with high *in vivo* potency do not necessarily show good performance *in vitro*, with AAV8, AAV9, and AAV-PHP.eB being only three of several nameable examples. Our previously published barcode-based mouse study[14] provides biodistribution data for most of the herein tested AAV variants after i.v. administration and can therefore serve as a source for comparative *in vitro–in vivo* assessment.

Finally, while we suggest AAV2.NN, AAV9-SLRSPPS, AAV6.2, AAV6TM, and AAV1P5 as a sufficient AAV core panel for the identification of powerful capsids for *in vitro/ex vivo* use, this selection could also be modified, for example, by replacing AAV1P5 with AAV9A2 or AAV-LK03, with the latter showing particularly strong expression in iPSCs, whereas AAV1P5 and AAV9A2 both appeared as the top hit in certain different cell types, but still showed a similar overall transduction pattern. Of note, while also other capsids, including those that were previously shown to be efficient *in vitro*, including AAV2-7m8 or AAV-Kera2, demonstrated overall good efficiencies, they were still constantly outperformed by one or more of the selected core panel variants.

CONCLUSION

We established a 96-well-based panel comprising 50 of the most used AAV variants to date, which allowed the identification of potent capsid variants for the transduction of various primary cells and cell lines, with a particular focus on human origin. Besides enabling the rapid identification of powerful tool vectors for cellular experiments, our data also shed light on cell-type-specific or conditional transduction patterns of certain AAV variants, which might be of use for capsid characterization or capsid engineering approaches. Importantly, our data demonstrate that a core panel comprising AAV2.NN, AAV9-SLRSPPS, AAV6.2, AAV6TM, and AAV1P5 is sufficient to identify highly potent capsids for *in vitro/ex vivo* use in all tested cell types. These findings will be of great practical value for early research applications, where AAV vectors are used as tools to modulate gene expression to study pathway biology, validate targets, or develop advanced screening assays.

ACKNOWLEDGMENTS

The authors greatly thank all the colleagues from Boehringer Ingelheim's research departments who provided cells for AAV transduction assessment and Dietmar Haag (Boehringer Ingelheim IT) for deploying the web app. We also thank Julia Dörner for conceptual contributions to the siRNA experiment.

AUTHORS' CONTRIBUTIONS

J.W.: conceptualization, methodology, investigation, formal analysis, visualization, and writing—original draft; J.S.: software; S.A., G.Z., K.Z., C.M., and J.D.-L.: investigation and formal analysis; A.P.: software; M.S.: methodology, investigation, and formal analysis; T.L.: conceptualization, methodology, investigation, project administration, and supervision; B.S.: conceptualization, methodology, investigation, formal analysis, project administration, supervision, visualization, and writing—original draft.

AUTHOR DISCLOSURE

All authors are employees of Boehringer Ingelheim Pharma GmbH & Co. KG.

FUNDING INFORMATION

This work was funded by Boehringer Ingelheim Pharma GmbH & Co. KG.

SUPPLEMENTARY MATERIAL

Supplementary Data
Supplementary Figure S1

REFERENCES

1. Girod A, Ried M, Wobus C, et al. Genetic capsid modifications allow efficient re-targeting of adeno-associated virus type 2. Nat Med 1999; 5(9):1052–1056; doi: 10.1038/12491

2. Grifman M, Trepel M, Speece P, et al. Incorporation of tumor-targeting peptides into recombinant adeno-associated virus capsids. Mol Ther 2001;3(6): 964–975; doi: 10.1006/mthe.2001.0345

3. Nicklin SA, Buening H, Dishart KL, et al. Efficient and selective AAV2-mediated gene transfer directed to human vascular endothelial cells. Mol Ther 2001; 4(3):174–181; doi: 10.1006/mthe.2001.0424

4. Perabo L, Büning H, Kofler DM, et al. In vitro selection of viral vectors with modified tropism: The adeno-associated virus display. Mol Ther 2003;8(1):151–157.
5. Müller OJ, Kaul F, Weitzman MD, et al. Random peptide libraries displayed on adeno-associated virus to select for targeted gene therapy vectors. Nat Biotechnol 2003;21(9):1040–1046; doi: 10.1038/nbt856
6. Work LM, Nicklin SA, Brain NJR, et al. Development of efficient viral vectors selective for vascular smooth muscle cells. Mol Ther 2004;9(2): 198–208; doi: 10.1016/j.ymthe.2003.11.006
7. Waterkamp DA, Müller OJ, Ying Y, et al. Isolation of targeted AAV2 vectors from novel virus display libraries. J Gene Med 2006;8(11):1307–1319; doi: 10.1002/jgm.967
8. Michelfelder S, Lee M-K, deLima-Hahn E, et al. Vectors selected from adeno-associated viral display peptide libraries for leukemia cell–targeted cytotoxic gene therapy. Exp Hematol 2007;35(12): 1766–1776; doi: 10.1016/j.exphem.2007.07.018
9. Sellner L, Stiefelhagen M, Kleinschmidt JA, et al. Generation of efficient human blood progenitor–targeted recombinant adeno-associated viral vectors (AAV) by applying an AAV random peptide library on primary human hematopoietic progenitor cells. Exp Hematol 2008;36(8):957–964; doi: 10.1016/j.exphem.2008.03.007
10. Stiefelhagen M, Sellner L, Kleinschmidt JA, et al. Application of a haematopoetic progenitor cell-targeted adeno-associated viral (AAV) vector established by selection of an AAV random peptide library on a leukaemia cell line. Genetic Vaccines Ther 2008;6(1):12; doi: 10.1186/1479-0556-6-12
11. Zhong L, Li B, Mah CS, et al. Next generation of adeno-associated virus 2 vectors: Point mutations in tyrosines lead to high-efficiency transduction at lower doses. Proc Natl Acad Sci U S A 2008; 105(22):7827–7832; doi: 10.1073/pnas.0802866105
12. Deverman BE, Pravdo PL, Simpson BP, et al. Cre-dependent selection yields AAV variants for widespread gene transfer to the adult brain. Nat Biotechnol 2016;34(2):204–209; doi: 10.1038/nbt.3440
13. Dalkara D, Byrne LC, Klimczak RR, et al. In vivo-directed evolution of a new adeno-associated virus for therapeutic outer retinal gene delivery from the vitreous. Sci Transl Med 2013;5(189): 189ra76; doi: 10.1126/scitranslmed.3005708
14. Weinmann J, Weis S, Sippel J, et al. Identification of a myotropic AAV by massively parallel in vivo evaluation of barcoded capsid variants. Nat Commun 2020;11(1):5432; doi: 10.1038/s41467-020-19230-w
15. Lisowski L, Dane AP, Chu K, et al. Selection and evaluation of clinically relevant AAV variants in a xenograft liver model. Nature 2014;506(7488): 382–386; doi: 10.1038/nature12875
16. Tabebordbar M, Lagerborg KA, Stanton A, et al. Directed evolution of a family of AAV capsid variants enabling potent muscle-directed gene delivery across species. Cell 2021;184(19):4919.e22–4938.e22; doi: 10.1016/j.cell.2021.08.028
17. Goertsen D, Flytzanis NC, Goeden N, et al. AAV capsid variants with brain-wide transgene expression and decreased liver targeting after intravenous delivery in mouse and marmoset. Nat Neurosci 2022; 25(1):106–115; doi: 10.1038/s41593-021-00969-4
18. Ellis BL, Hirsch ML, Barker JC, et al. A survey of ex vivo/in vitro transduction efficiency of mammalian primary cells and cell lines with nine natural adeno-associated virus (AAV1–9) and one engineered adeno-associated virus serotype. Virol J 2013;10(1):74; doi: 10.1186/1743-422x-10-74
19. Duong TT, Lim J, Vasireddy V, et al. Comparative AAV-EGFP transgene expression using vector serotypes 1–9, 7m8, and 8b in human pluripotent stem cells, RPEs, and human and rat cortical neurons. Stem Cells Int 2019;2019:7281912; doi: 10.1155/2019/7281912
20. Börner K, Kienle E, Huang L-Y, et al. Pre-arrayed pan-AAV peptide display libraries for rapid single-round screening. Mol Ther 2020;28(4):1016–1032; doi: 10.1016/j.ymthe.2020.02.009
21. Westhaus A, Cabanes-Creus M, Rybicki A, et al. High-throughput in vitro, ex vivo, and in vivo screen of adeno-associated virus vectors based on physical and functional transduction. Hum Gene Ther 2020; 31(9–10):575–589; doi: 10.1089/hum.2019.264
22. Strobel B, Zuckschwerdt K, Zimmermann G, et al. Standardized, scalable, and timely flexible adeno-associated virus vector production using frozen high-density HEK-293 cell stocks and CELLdiscs. Hum Gene Ther Method 2019;30(1):23–33; doi: 10.1089/hgtb.2018.228
23. Limb GA, Salt TE, Munro PMG, et al. In vitro characterization of a spontaneously immortalized human Müller cell line (MIO-M1). Invest Ophthalmol Vis Sci 2002;43(3):864–869.
24. Matsumoto T, Kano K, Kondo D, et al. Mature adipocyte-derived dedifferentiated fat cells exhibit multilineage potential. J Cell Physiol 2008; 215(1):210–222; doi: 10.1002/jcp.21304
25. Weigle S, Martin E, Voegtle A, et al. Primary cell-based phenotypic assays to pharmacologically and genetically study fibrotic diseases in vitro. J Biol Methods 2019;6(2):e115; doi: 10.14440/jbm.2019.285
26. Vandenberghe LH, Xiao R, Lock M, et al. Efficient serotype-dependent release of functional vector into the culture medium during adeno-associated virus manufacturing. Hum Gene Ther 2010;21(10): 1251–1257; doi: 10.1089/hum.2010.107
27. Xie J, Mao Q, Tai PWL, et al. Short DNA hairpins compromise recombinant adeno-associated virus genome homogeneity. Mol Ther 2017;25(6):1363–1374; doi: 10.1016/j.ymthe.2017.03.028
28. Tai PWL, Xie J, Fong K, et al. Adeno-associated virus genome population sequencing achieves full vector genome resolution and reveals human-vector chimeras. Mol Ther Methods Clin Dev 2018;9:130–141; doi: 10.1016/j.omtm.2018.02.002
29. Tran NT, Heiner C, Weber K, et al. AAV-genome population sequencing of vectors packaging CRISPR components reveals design-influenced heterogeneity. Mol Ther Methods Clin Dev 2020; 18:639–651; doi: 10.1016/j.omtm.2020.07.007
30. Rayaprolu V, Kruse S, Kant R, et al. Comparative analysis of adeno-associated virus capsid stability and dynamics. J Virol 2013;87(24):13150–13160; doi: 10.1128/jvi.01415-13
31. Vliet KV, Blouin V, Agbandje-McKenna M, et al. Proteolytic mapping of the adeno-associated virus capsid. Mol Ther 2006;14(6):809–821; doi: 10.1016/j.ymthe.2006.08.1222
32. Galibert L, Savy A, Dickx Y, et al. Origins of truncated supplementary capsid proteins in RAAV8 vectors produced with the baculovirus system. PLoS One 2018; 13(11):e0207414; doi: 10.1371/journal.pone.0207414
33. Bennett A, Patel S, Mietzsch M, et al. Thermal stability as a determinant of AAV serotype identity. Mol Ther Methods Clin Dev 2017;6:171–182; doi: 10.1016/j.omtm.2017.07.003
34. Pacouret S, Bouzelha M, Shelke R, et al. AAV-ID: A rapid and robust assay for batch-to-batch consistency evaluation of AAV preparations. Mol Ther 2017;25(6): 1375–1386; doi: 10.1016/j.ymthe.2017.04.001
35. Pavlou M, Schön C, Occelli LM, et al. Novel AAV capsids for intravitreal gene therapy of photoreceptor disorders. EMBO Mol Med 2021;13(4): e13392; doi: 10.15252/emmm.202013392
36. Rossi A, Dupaty L, Aillot L, et al. Vector uncoating limits adeno-associated viral vector-mediated transduction of human dendritic cells and vector immunogenicity. Sci Rep 2019;9(1):3631; doi: 10.1038/s41598-019-40071-1
37. Naumer M, Popa-Wagner R, Kleinschmidt JA. Impact of capsid modifications by selected peptide ligands on RAAV2-mediated gene transduction. J Gen Virol 2012; 93(Pt_10):2131–2141; doi: 10.1099/vir.0.044735-0
38. Drouin LM, Lins B, Janssen M, et al. Cryo-electron microscopy reconstruction and stability studies of the wild type and the R432A variant of adeno-associated virus type 2 reveal that capsid structural stability is a major factor in genome packaging. J Virol 2016;90(19): 8542–8551; doi: 10.1128/jvi.00575-16
39. Limberis MP, Vandenberghe LH, Zhang L, et al. Transduction efficiencies of novel AAV vectors in mouse airway epithelium in vivo and human ciliated airway epithelium in vitro. Mol Ther 2008; 17(2):294–301; doi: 10.1038/mt.2008.261
40. Strobel B, Duechs MJ, Schmid R, et al. Modeling pulmonary disease pathways using recombinant adeno-associated virus 6.2. Am J Resp Cell Mol 2015; 53(3):291–302; doi: 10.1165/rcmb.2014-0338ma
41. Ling C, Bhukhai K, Yin Z, et al. High-efficiency transduction of primary human hematopoietic stem/progenitor cells by AAV6 vectors: Strategies for overcoming donor-variation and implications in genome editing. Sci Rep 2016;6(1):35495; doi: 10.1038/srep35495
42. Balaz M, Becker AS, Balazova L, et al. Inhibition of mevalonate pathway prevents adipocyte browning in mice and men by affecting protein prenylation. Cell Metab 2019;29(4):901.e8–916.e8; doi: 10.1016/j.cmet.2018.11.017
43. Varadi K, Michelfelder S, Korff T, et al. Novel random peptide libraries displayed on AAV serotype 9 for selection of endothelial cell-directed

gene transfer vectors. Gene Ther 2012;19(8):800–809; doi: 10.1038/gt.2011.143

44. Li S, Ling C, Zhong L, et al. Efficient and targeted transduction of nonhuman primate liver with systemically delivered optimized AAV3B vectors. Mol Ther 2015;23(12):1867–1876; doi: 10.1038/mt.2015.174

45. Paulk NK, Pekrun K, Zhu E, et al. Bioengineered AAV capsids with combined high human liver transduction in vivo and unique humoral seroreactivity. Mol Ther 2018;26(1):289–303; doi: 10.1016/j.ymthe.2017.09.021

46. Dudek AM, Pillay S, Puschnik AS, et al. An alternate route for adeno-associated virus (AAV) entry independent of AAV receptor. J Virol 2018; 92(7):e02213-17; doi: 10.1128/jvi.02213-17

47. Nicolson SC, Li C, Hirsch ML, et al. Identification and validation of small molecules that enhance recombinant adeno-associated virus transduction following high-throughput screens. J Virol 2015; 90(16):7019–7031; doi: 10.1128/jvi.02953-15

48. Swanson JA. Phorbol esters stimulate macropinocytosis and solute flow through macrophages. J Cell Sci 1989;94(1):135–142; doi: 10.1242/jcs.94.1.135

49. Weinberg MS, Nicolson S, Bhatt AP, et al. Recombinant adeno-associated virus utilizes cell-specific infectious entry mechanisms. J Virol 2014; 88(21):12472–12484; doi: 10.1128/jvi.01971-14

50. Chiang DJ, Pritchard MT, Nagy LE. Obesity, diabetes mellitus, and liver fibrosis. Am J Physiol Gastrointest Liver Physiol 2011;300(5):G697–G702; doi: 10.1152/ajpgi.00426.2010

51. Aumiller V, Strobel B, Romeike M, et al. Comparative analysis of lysyl oxidase (like) family members in pulmonary fibrosis. Sci Rep 2017;7(1): 149; doi: 10.1038/s41598-017-00270-0

52. Zinn E, Pacouret S, Khaychuk V, et al. In silico reconstruction of the viral evolutionary lineage yields a potent gene therapy vector. Cell Rep 2015; 12(6):1056–1068; doi: 10.1016/j.celrep.2015.07.019

53. Hoggan MD, Blacklow NR, Rowe WP. Studies of small DNA viruses found in various adenovirus preparations: Physical, biological, and immunological characteristics. Proc Natl Acad Sci U S A 1966;55(6):1467–1474.

54. Cronin T, Vandenberghe LH, Hantz P, et al. Efficient transduction and optogenetic stimulation of retinal bipolar cells by a synthetic adeno-associated virus capsid and promoter. EMBO Mol Med 2014;6(9): 1175–1190; doi: 10.15252/emmm.201404077

55. Gao G, Vandenberghe LH, Alvira MR, et al. Clades of adeno-associated viruses are widely disseminated in human tissues. J Virol 2004;78(12):6381–6388; doi: 10.1128/jvi.78.12.6381-6388.2004

56. Hanlon KS, Meltzer JC, Buzhdygan T, et al. Selection of an efficient AAV vector for robust CNS transgene expression. Mol Ther Methods Clin Dev 2019;15:320–332; doi: 10.1016/j.omtm.2019.10.007

57. Opie SR, Warrington, KH, Agbandje-McKenna M, et al. Identification of amino acid residues in the capsid proteins of adeno-associated virus type 2 that contribute to heparan sulfate proteoglycan binding. J Virol 2003;77(12):6995–7006; doi: 10.1128/jvi.77.12.6995-7006.2003

58. Aslanidi GV, Rivers AE, Ortiz L, et al. Optimization of the capsid of recombinant adeno-associated virus 2 (AAV2) vectors: The final threshold? PLoS One 2013; 8(3):e59142; doi:10.1371/journal.pone.0059142

59. Chan KY, Jang MJ, Yoo BB, et al. Engineered AAVs for efficient noninvasive gene delivery to the central and peripheral nervous systems. Nat Neurosci 2017;20(8):1172–1179; doi: 10.1038/nn.4593

60. Yu C-Y, Yuan Z, Cao Z, et al. A muscle-targeting peptide displayed on AAV2 improves muscle tropism on systemic delivery. Gene Ther 2009;16(8): 953–962; doi: 10.1038/gt.2009.59

61. Schmidt M, Voutetakis A, Afione S, et al. Adeno-associated virus type 12 (AAV12): A novel AAV serotype with sialic acid- and heparan sulfate proteoglycan-independent transduction activity. J Virol 2007;82(3):1399–1406; doi: 10.1128/jvi.02012-07

62. Bello A, Tran K, Chand A, et al. Isolation and evaluation of novel adeno-associated virus sequences from porcine tissues. Gene Ther 2009; 16(11):1320–1328; doi: 10.1038/gt.2009.82

63. Körbelin J, Sieber T, Michelfelder S, et al. Pulmonary targeting of adeno-associated viral vectors by next-generation sequencing-guided screening of random capsid displayed peptide libraries. Mol Ther 2016;24(6):1050–1061; doi: 10.1038/mt.2016.62

64. Vandenberghe LH, Breous E, Nam HJ, et al. Naturally occurring singleton residues in AAV capsid impact vector performance and illustrate structural constraints. Gene Ther 2009;16(12): 1416–1428; doi: 10.1038/gt.2009.101

65. Sallach J, Pasquale GD, Larcher F, et al. Tropism-modified AAV vectors overcome barriers to successful cutaneous therapy. Mol Ther 2014;22(5): 929–939; doi: 10.1038/mt.2014.14

66. Mendell JR, Chicoine L, Rodino-Klapac L, et al. Recombinant adeno-associated virus delivery of alpha-sarcoglycan polynucleotides. Patent Application no: WO2013078316A1

67. Tervo DGR, Hwang B-Y, Viswanathan S, et al. A designer AAV variant permits efficient retrograde access to projection neurons. Neuron 2016;92(2): 372–382; doi: 10.1016/j.neuron.2016.09.021

68. Rutledge EA, Halbert CL, Russell DW. Infectious clones and vectors derived from adeno-associated virus (AAV) serotypes other than AAV type 2. J Virol 1998;72:309–319.

69. Choudhury SR, Fitzpatrick Z, Harris AF, et al. In vivo selection yields AAV-B1 capsid for central nervous system and muscle gene therapy. Mol Ther 2016; 24(7):1247–1257; doi: 10.1038/mt.2016.84

70. Parks WP, Melnick JL, Rongey R, et al. Physical assay and growth cycle studies of a defective adeno-satellite virus. J Virol 1967;1(1):171–180; doi: 10.1128/jvi.1.1.171-180.1967

71. Grimm D, Lee JS, Wang L, et al. In vitro and in vivo gene therapy vector evolution via multispecies interbreeding and retargeting of adeno-associated viruses. J Virol 2008;82(12):5887–5911; doi: 10.1128/jvi.00254-08

72. Bantel-Schaal U, Hausen HZ. Characterization of the DNA of a defective human parvovirus isolated from a genital site. Virology 1984;134(1):52–63; doi: 10.1016/0042-6822(84)90271-x

73. Yang L, Jiang J, Drouin LM, et al. A myocardium tropic adeno-associated virus (AAV) evolved by DNA shuffling and in vivo selection. Proc Natl Acad Sci U S A 2009;106(10):3946–3951; doi: 10.1073/pnas.0813207106

74. Paulk NK, Pekrun K, Charville GW, et al. Bioengineered viral platform for intramuscular passive vaccine delivery to human skeletal muscle. Mol Ther Methods Clin Dev 2018;10:144–155; doi: 10.1016/j.omtm.2018.06.001

75. van Lieshout LP, Domm JM, Rindler TN, et al. A novel triple-mutant AAV6 capsid induces rapid and potent transgene expression in the muscle and respiratory tract of mice. Mol Ther Methods Clin Dev 2018;9:323–329; doi: 10.1016/j.omtm.2018.04.005

76. Powell SK, Khan N, Parker CL, et al. Characterization of a novel adeno-associated viral vector with preferential oligodendrocyte tropism. Gene Ther 2016;23(11):807–814; doi: 10.1038/gt.2016.62

77. Ojala DS, Sun S, Santiago-Ortiz JL, et al. In vivo selection of a computationally designed SCHEMA AAV library yields a novel variant for infection of adult neural stem cells in the SVZ. Mol Ther 2018; 26(1):304–319; doi: 10.1016/j.ymthe.2017.09.006

78. Gao GP. Novel adeno-associated viruses from rhesus monkeys as vectors for human gene therapy. Proc Natl Acad Sci U S A 2002;99(18):11854–11859; doi: 10.1073/pnas.182412299

79. Klimczak RR, Koerber JT, Dalkara D, et al. A novel adeno-associated viral variant for efficient and selective intravitreal transduction of rat Müller cells. PLoS One 2009;4(10):e7467; doi: 10.1371/journal.pone.0007467

Received for publication May 8, 2022;
accepted after revision September 7, 2022.

Published online: September 12, 2022.